On Use of Positive Feedback for Improved Torque Control

Houman Dallali, Gustavo A. Medrano-Cerda,
Michele Focchi, Thiago Boaventura, Marco Frigerio,
Claudio Semini, Jonas Buchli, and Darwin G. Caldwell, ‡

September 25, 2014

Abstract

This paper considers the torque control problem for robots with flexible joints driven by electrical actuators. It is shown that the achievable closed loop tracking bandwidth using PI torque controllers may be limited due to transmission zeros introduced by the load dynamics. This limitation is overcome by using positive feedback from the load motion in unison with PI torque controllers. The positive feedback is given in terms of load velocity, acceleration and jerk. Stability conditions for designing decentralized PI torque controllers are derived in terms of Routh-Hurwitz criteria. Disturbance rejection properties of the closed system are characterized and an analysis is carried out investigating the use of approximate positive feedback by omitting acceleration and/or jerk signals. The results of this paper are illustrated for a two DoF system. Experimental results for a one DoF system are also included.

1 Introduction

Enhancing the bandwidth of torque tracking is one of the challenges in building high performance legged robots. The problem of increasing the torque bandwidth cannot be resolved by using faster actuators but it is related to the load motion rather than the actuator dynamics. This issue becomes more critical when the load has little friction, i.e. good bearings are used at the point where the load is attached to the transmission. In the robotics community, many publications on torque control have disregarded the load dynamics from the analysis [1, 2, 3] and this problem has been overlooked.

*H Dallali, G. A. Medrano-Cerda, M. Focchi, M. Frigerio, C. Semini and D. G. Caldwell are with the Department of Advanced Robotics, Istituto Italiano di Tecnologia (IIT), Genova, Italy.

†T. Boaventura and J. Buchli are with Agile and Dexterous Robotics Lab, Institute of Robotics and Intelligent Systems, ETH, Zürich, Switzerland.

‡Manuscript received September 25, 2014.

However bandwidth limitations in force control problems using hydraulic actuators have been reported in civil and automotive engineering. In [4] the interaction between the load motion and the actuator was shown for a hydraulic actuator. It was shown that a natural velocity feedback interaction path exists between the load (in that case a civil structure) and the actuator. Moreover, using a linearized model it was shown that the poles of the structure become the zeros of the open loop force transfer function. As a result, if the structure is lightly damped, the actuators will be unable to apply a force at the natural frequency of the structure, regardless of actuator dynamics speed (bandwidth). In [4] it was shown that the problem is not due to the actuator dynamics but due to the structure (load) dynamics. In [5], experimental results of a car suspension test rig were reported where a conventional PID controller was incapable of producing appropriate force tracking and resulted in a significant phase lag at frequencies higher than 1 Hz. The car test rig used very fast servo-valve dynamics to improve the force tracking performance but the problem was not resolved. In [6], the interaction between the hydraulic actuator and the structure is discussed and an intuitive positive velocity feedback scheme is proposed to compensate for the load motion by negating the effect of the natural velocity feedback. Despite simulation studies and experimental results, further analysis details on the effect of adding the positive feedback loop were not presented. Later in [7], several improvements were made to this method including the addition of phase adjustment to the positive velocity feedback. Also the magnitude of the positive velocity feedback was underestimated to avoid potential instability. In [8] motor torque control was considered using a disturbance observer while no load was attached to the motor. In this work we are interested in torque control at the joint and a system where the inertia is coupled via a compliant joint. In [9], the authors showed how motion compensation can be applied to electrically and hydraulically actuated joints of a quadruped robot called HyQ [10]. In [11], positive torque feedback was used to improve the problem of joint tracking, but it does not report the load motion problem. It was reported that positive joint torque feedback can compensate the detrimental effects of load torques on position tracking performance. However, with non-ideal torque sources, simple unity gain positive torque feedback can actually deteriorate the performance, or even result in instability.

Various complex control designs can be used for torque control. For instance, in [12] a combination of model based computed torque control, a state feedback and a nonlinear H_∞ was applied to a six DoF robot manipulator with joint flexibility. A high performance torque control method was implemented on a light weight robot arm in [13]. These methods need a good model and are implemented in centralized architectures which places additional requirements on real-time communication among various Degrees of Freedom (DoF).

In practice, the use of decentralized PI controllers is widespread in robotics. PI controllers are easy to tune but have limitations in terms of tracking bandwidth and disturbance rejection. The main idea in this paper is to use decentralized controllers by mitigating the existing limitations using quantified positive feedback. The source of these limitations will be fully characterized for

multi-dof systems in terms of multi-variable zeros.

The main contributions of this paper are the following: The role of positive feedback is studied for mechanical systems driven with electric motors. It is shown that simple PI controllers can be used together with positive feedback to significantly improve torque tracking performance. Stability conditions for designing decentralized PI torque controllers, when the positive feedback is applied, are presented in terms of Routh-Hurwitz criteria. A two DoF case study is used to illustrate the theory via root locus analysis and numerical simulations. Experimental results of a one DoF system are presented, validating the use of positive feedback.

The paper is organized as follows. Section 2, presents the system model and characterizes the corresponding multi-variable transmission zeros. Limitations on the achievable closed loop torque bandwidth are explained in terms of the transmission zeros when using simple PI controllers. The use of positive feedback is introduced and it is shown that this can be designed to decouple the joint torque from the load dynamics. The positive feedback is given by three terms involving load velocity, acceleration and jerk. General results to investigate closed loop stability when using this method are presented in section 2.4. Section 2.5, discusses disturbance rejection properties of the closed loop system and in particular points out additional limitations when using PI torque controllers. In section 3, a case study based on a two DoF model is used to verify the main results via nonlinear simulations and root locus analysis. In particular, the root locus analysis in section 3.4 investigates the effects of using a partial positive feedback by neglecting load acceleration and/or jerk terms. Section 4 presents some experimental results for one joint of a robot leg prototype [14]. Concluding remarks are given in section 5.

Notation Throughout the paper, lower case letters are used for scalars, lower case and bold letters are used for vectors and uppercase letters are used for matrices. Moreover, subscripts L and m refer to load and motor, respectively.

2 System Model and Main Results

This section presents the main results of the paper for the multi-Dof system given by

$$M_L(\boldsymbol{\theta}_L)\ddot{\boldsymbol{\theta}}_L + C_L(\dot{\boldsymbol{\theta}}_L, \boldsymbol{\theta}_L) + B_L\dot{\boldsymbol{\theta}}_L + G(\boldsymbol{\theta}_L) = \boldsymbol{\tau}_L + \boldsymbol{\tau_{Ld}}, \tag{1}$$

$$J_m\ddot{\boldsymbol{\theta}}_m + B_m\dot{\boldsymbol{\theta}}_m + N^{-1}\boldsymbol{\tau}_L = K_t\boldsymbol{i} + N^{-1}\boldsymbol{\tau_d}, \tag{2}$$

$$L\dot{\boldsymbol{i}} + R\boldsymbol{i} = \boldsymbol{v_m} - K_\omega\dot{\boldsymbol{\theta}}_m, \tag{3}$$

$$\boldsymbol{\tau}_L = K_H\left(N^{-1}\boldsymbol{\theta}_m - \boldsymbol{\theta}_L\right), \tag{4}$$

where $\boldsymbol{\theta}_L$, $\boldsymbol{\theta}_m$, $\dot{\boldsymbol{\theta}}_L$, $\dot{\boldsymbol{\theta}}_m$ are the angular positions and velocities of the load and motor in relative coordinates; $\boldsymbol{\tau}_L$ denotes the joint torque; $\boldsymbol{\tau_{Ld}}$, $\boldsymbol{\tau_d}$ are disturbances acting on the link and motor; $\boldsymbol{i}$ and $\boldsymbol{v_m}$ are the motors current

and voltage, respectively. The motor disturbance $\boldsymbol{\tau_d}$ can represent meshing friction and torque ripples produced by a reduction gearbox. We assume that the joint torque $\boldsymbol{\tau_L}$, the load and the motor positions are measured. Note however that one set of measurements is redundant since (4) provides a relation between them. A description of the system parameters is summarized in Table 1. The motor equations in the model correspond to a DC permanent magnet motor but as indicated by several motor manufacturers the same equations can be used for DC brushless motors whenever these are appropriately commutated. Linearizing (1) at a given load position with zero angular velocity yields

$$M_L\ddot{\boldsymbol{\theta}}_L + B_L\dot{\boldsymbol{\theta}}_L + K_L\boldsymbol{\theta}_L = \boldsymbol{\tau}_L. \tag{5}$$

where M_L is obtained by evaluating the mass inertia matrix at a given load position and the linearized gravity vector K_L is obtained by evaluating the partial derivative of G at the given robot configuration.

Throughout the paper, the linearized model is used to investigate stability and disturbance rejection properties of the closed loop system when a PI torque controller is combined with positive feedback. The linearized analysis can be easily repeated for several configurations of interest by generating a suitable mesh of the robot workspace. In this manner the closed loop performance of the robot can be investigated at different robot configurations. A case study will illustrate that the predicted performance using the linearized analysis can be reasonably close to the results obtained via nonlinear simulations. The following result presents an important property of the linearized system.

Lemma 1 Multi-variable Transmission Zeros
Consider the linearized system given by (5), (2)-(4) *and define*
$\Lambda_L(s) = M_L s^2 + B_L s + K_L$.
The transmission zeros from the motor voltage to the joint torque are given by the roots of the polynomial $det(\Lambda_L(s)) = 0$.

Proof: See Appendix 6.
Lemma 1 has substantial implications on the achievable closed loop performance of a torque control system when using PI torque controllers. Consider the case when B_L and K_L are positive definite matrices then the transmission zeros lie in the left half plane. If the damping B_L is very small then these zeros will be close to the imaginary axis and the PI controller poles at the origin will be attracted towards these zeros. Hence closed loop poles near the imaginary axis arise and these poles have slow transients therefore the closed loop system has a low bandwidth. These effects will be illustrated in section 3.2 for a two DoF example. When K_L is not positive definite then some transmission zeros appear in the right half plane (non-minimum phase zeros). In addition, in this case the open loop system is also unstable. In general this type of systems are more difficult to control [15] and further discussions are given for the two DoF case study in a later section.

Table 1: The System Parameters

Parameter	Description	Parameter	Description	Parameter	Description
J_m	Motor & gearbox inertia	R	Motor resistance	M_L	Mass-inertia matrix
K_t	Torque-current constant	B_m	Motor Damping	C_L	Coriolis & centrifugal force vector
K_ω	Back-emf constant	L	Motor Inductance	G	Gravity vector
K_H	Transmission stiffness	N	Reduction ratio	K_L	Linearized gravity matrix
B_L	Joint Damping	-	-	-	

2.1 *Positive Feedback Compensation*

This section introduces the idea of positive feedback compensation and shows how by suitable design, it can decouple the load motion from the joint torque dynamics.

Lemma 2 *Consider the linearized system* (5), (2)-(4) *and introduce the feedback* $\boldsymbol{v_m} = F(s)\boldsymbol{\theta_L} + \boldsymbol{v_r}$, *where* $\boldsymbol{v}_r$ *is the reference voltage. The corresponding linear closed loop system is given by*

$$\begin{bmatrix} Q(s) & Y(s) \\ -I & \Lambda_L(s) \end{bmatrix} \begin{bmatrix} \boldsymbol{\tau}_L \\ \boldsymbol{\theta}_L \end{bmatrix} = \begin{bmatrix} \boldsymbol{v}_r \\ 0 \end{bmatrix} + \begin{bmatrix} (Ls+R)K_t^{-1}\boldsymbol{\tau}_d \\ \boldsymbol{\tau_{Ld}} \end{bmatrix} \tag{6}$$

where I *is an identity matrix and*

$$\begin{aligned} Q(s) &= ((Ls+R)K_t^{-1}\Lambda_1(s) + K_\omega s)NK_H^{-1} \qquad (7)\\ &= A_3s^3 + A_2s^2 + A_1s + A_0 \\ Y(s) &= (Ls+R)K_t^{-1}\Lambda_m(s)N + K_\omega Ns - F(s) \qquad (8)\\ &= \Gamma_j s^3 + \Gamma_a s^2 + \Gamma_v s - F(s) \\ \Lambda_m(s) &= J_m s^2 + B_m s, \quad \Lambda_1(s) = \Lambda_m(s) + N^{-1}K_H N^{-1}. \qquad (9) \end{aligned}$$

where

$$\Gamma_j = LK_t^{-1}J_mN,\ \Gamma_a = LK_t^{-1}B_mN + RK_t^{-1}J_mN,\ \Gamma_v = RK_t^{-1}B_mN + K_\omega N, \tag{10}$$

and

$$A_3 = \Gamma_j K_H^{-1},\quad A_2 = \Gamma_a K_H^{-1},\quad A_1 = \Gamma_v K_H^{-1} + LK_t^{-1}N^{-1},\ A_0 = RK_t^{-1}N^{-1}. \tag{11}$$

Proof: See Appendix 7.
A block diagram representation of (6) is shown in Fig.1. Inside the dashed box we have the intrinsic feedback in the system and the outer positive feedback loop can be chosen to cancel out the intrinsic feedback. From Lemma 2 by selecting $F(s)$ such that $Y(s) = 0$, the joint torque $\boldsymbol{\tau_L}$ is decoupled from the load dynamics.

Lemma 3 Positive feedback compensation
The feedback

$$\boldsymbol{v_m} = \Gamma_j \boldsymbol{\theta_L^{(3)}} + \Gamma_a \ddot{\boldsymbol{\theta}}_{\boldsymbol{L}} + \Gamma_v \dot{\boldsymbol{\theta}}_{\boldsymbol{L}} + \boldsymbol{v_r} \tag{12}$$

Decouples the joint torque $\boldsymbol{\tau_L}$ *from the load dynamics.*

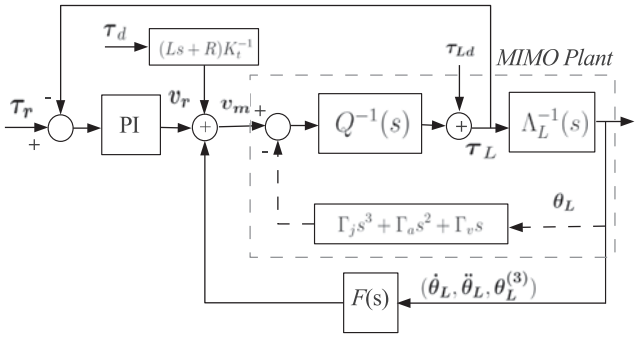

Figure 1: Control block diagram for linearized system, where $\boldsymbol{\tau_r}$ denotes the input reference torque, $F(s)$ is the positive velocity feedback gain.

Proof. This is a direct consequence of Lemma 2. Setting $Y(s) = 0$ in (6), solving for $F(s)$ and taking inverse Laplace transforms yields (12). ■
Note that in (6) the matrix on the left hand side becomes lower triangular for the feedback (12) since $Y(s) = 0$. This implies that the load dynamics are unobservable from the joint torque and the multivariable transmission zeros are cancelled by the load dynamic poles.

In addition, the feedback compensation (12) only depends on the drives parameters and since these matrices are diagonal (12) is a decentralized feedback assuming that the velocities, acceleration and jerk signals are available. Furthermore, the matrix $Q(s)$ is also a diagonal matrix that only depends on the drive parameters.

Remark 1: The results in Lemmas 2 and 3 can be obtained without using the linearized equation (5). The derivation can be carried out entirely in the time domain but becomes a little more elaborate. Therefore for the nonlinear system, the positive feedback compensation (12) also decouples the joint torque $\boldsymbol{\tau_L}$ from the load dynamics.
The next section considers the design of a PI torque controller.

2.2 *PI Control and Positive Feedback*

Once the feedback compensation is implemented we introduce a decentralized PI torque controller given by

$$\boldsymbol{v_r} = K_p(I + \frac{K_i}{s})(\boldsymbol{\tau_r} - \boldsymbol{\tau_L}) \tag{13}$$

where K_p, K_i are diagonal matrices, and $\boldsymbol{\tau_r}$ is the reference torque.

Lemma 4 *Consider the system in Lemma 2 and the PI torque controller* (13). *The closed loop system is*

$$\begin{bmatrix} Q_c(s) & Y(s)s \\ -I & \Lambda_L(s) \end{bmatrix} \begin{bmatrix} \boldsymbol{\tau}_L \\ \boldsymbol{\theta}_L \end{bmatrix} = \begin{bmatrix} K_p(s+K_i)\boldsymbol{\tau}_r \\ 0 \end{bmatrix} + \begin{bmatrix} (Ls+R)K_t^{-1}\boldsymbol{\tau}_d \\ \boldsymbol{\tau_{Ld}} \end{bmatrix} \tag{14}$$

where

$$Q_c(s) = A_3 s^4 + A_2 s^3 + A_1 s^2 + (A_0 + K_p)s + K_p K_i. \tag{15}$$

Proof. From Lemma 2, substituting (13) in (6), the result follows after some standard algebraic calculations. ■

Lemma 4 will be used in subsequent sections to determine closed loop stability for any given PI controller and any feedback compensation as in Lemma 2.

2.3 *Implementation Requirements*

Implementation of the feedback compensation (12) requires velocity, acceleration and jerk signals which are not measured. In general, the acceleration and jerk feedback terms cannot be discarded since the system (14) can become unstable even if $Q_c(s)$ is asymptotically stable. A result for investigating stability when acceleration and/or jerk feedback are ignored is given in section 2.4 and further discussions are presented in section 3 for a two DoF example. In the experimental section 4, load's velocity, acceleration and jerk are computed online and used for full load motion compensation.

The velocity, acceleration and jerk signals required in (12) can be obtained via robust numerical differentiators. Relevant publications in this topic are [16], [17], and [18]. In [19] an application is considered where numerical differentiation is used to determine acceleration. In [20] the authors present a nonlinear velocity estimator. Reducing noise in the measurements can be accomplished using high resolution position encoders and filtering to obtain approximate derivatives, as used in the experimental results in section 4.

An alternative to numerical differentiation is to use the system model. From the nonlinear equation (1) we can obtain the load acceleration and jerk signals

$$\ddot{\boldsymbol{\theta}}_{\boldsymbol{L}} = M_L^{-1}(\boldsymbol{\theta}_L)(-C_L(\dot{\boldsymbol{\theta}}_{\boldsymbol{L}}, \boldsymbol{\theta}_L) - B_L\dot{\boldsymbol{\theta}}_{\boldsymbol{L}} - G(\boldsymbol{\theta}_{\boldsymbol{L}}) + \boldsymbol{\tau}_{\boldsymbol{L}}) \tag{16}$$

$$\boldsymbol{\theta}_{\boldsymbol{L}}^{(3)} = M_L^{-1}(\boldsymbol{\theta}_L)\left(-\dot{M}_L(\boldsymbol{\theta}_L)\ddot{\boldsymbol{\theta}}_{\boldsymbol{L}} - \dot{C}_L(\dot{\boldsymbol{\theta}}_L, \boldsymbol{\theta}_L) - B_L\ddot{\boldsymbol{\theta}}_L - \dot{G}(\boldsymbol{\theta}_L) + \dot{\boldsymbol{\tau}}_{\boldsymbol{L}}\right) \tag{17}$$

In (16)-(17) the load disturbance $\boldsymbol{\tau_{Ld}}$ has been neglected since this is not known. Neglecting the disturbance can have some degradation in performance but does not affect stability. Estimation of load acceleration and jerk also requires knowing the Coriolis, gravity and dynamic parameters of the system accurately. Furthermore (16) and (17) incorporate all the load interactions and can be implemented as a centralized scheme. For the linearized analysis acceleration and jerk signals can be computed from (5), also ignoring the load disturbance $\boldsymbol{\tau_{Ld}}$

$$\ddot{\boldsymbol{\theta}}_{\boldsymbol{L}} = M_L^{-1}(-B_L\dot{\boldsymbol{\theta}}_{\boldsymbol{L}} - K_L\boldsymbol{\theta}_{\boldsymbol{L}} + \boldsymbol{\tau}_{\boldsymbol{L}}) \tag{18}$$

$$\boldsymbol{\theta}_{\boldsymbol{L}}^{(3)} = M_L^{-1}\left(-B_L\ddot{\boldsymbol{\theta}}_L - K_L\dot{\boldsymbol{\theta}}_L + \dot{\boldsymbol{\tau}}_{\boldsymbol{L}}\right) \tag{19}$$

In this case (18)-(19) can also be written as feedback in terms of system states,($\boldsymbol{\theta_m}$, $\boldsymbol{\theta_L}$, $\dot{\boldsymbol{\theta}}_{\boldsymbol{m}}$ and $\dot{\boldsymbol{\theta}}_{\boldsymbol{L}}$) or ($\boldsymbol{\tau_L}$, $\boldsymbol{\theta_L}$, $\dot{\boldsymbol{\tau}}_{\boldsymbol{L}}$ and $\dot{\boldsymbol{\theta}}_{\boldsymbol{L}}$).

2.4 *Stability Analysis*

This section, first considers the stability of the closed loop system in Lemma 4 when the positive feedback compensation is chosen as in Lemma 3 so that $Y(s) = 0$. The second result in this section is derived to determine closed loop stability of the system when the positive feedback compensation is partially implemented.

Lemma 5 *Consider the closed loop system in lemma 4 with the feedback compensation in Lemma 3, then the closed loop torque response is given by*

$$Q_c(s)\boldsymbol{\tau_L} = K_p(s + K_i)\boldsymbol{\tau}_r + (Ls + R)K_t^{-1}s\boldsymbol{\tau_d}. \tag{20}$$

Proof. From (14) setting $Y(s) = 0$. ■
Since all the matrices in (20) are diagonal, the system reduces to a set of uncoupled single input single output systems and $Q_c(s) = \text{diag}(q_{c1}(s),\ q_{c2}(s),$ $..., q_{cn}(s))$ where each polynomial $q_{ci}(s) = a_{3i}s^4 + a_{2i}s^3 + a_{1i}s^2 + (a_{0i} + k_{pi})s + k_{pi}k_{ii}$ and all the scalars k_{pi}, k_{ii}, a_{3i}, a_{2i}, a_{1i} and a_{0i} are positive. From the Routh-Hurwitz array, conditions for stability of $Q_c(s)$ are

$$0 < k_{pi} < (\frac{a_{1i}a_{2i}}{a_{3i}} - a_{0i}) \ \text{ and} \tag{21}$$

$$0 < k_{ii} < \left(\frac{a_{1i}a_{2i}}{a_{3i}} - (a_{0i} + k_{pi})\right)\left(\frac{(a_{0i} + k_{pi})a_{3i}}{k_{pi}^2 a_{2i}^2}\right). \tag{22}$$

These inequalities give a range of values for the controller gains k_{pi} and k_{ii} ensuring closed loop stability.

The second result in this section is useful for investigating stability when the full compensation in Lemma 3 is not implemented for example to determine if the terms involving jerk and acceleration can be neglected.
Consider the PI torque controller (13) and the feedback compensation

$$\boldsymbol{v_m} = \alpha_j\Gamma_j\boldsymbol{\theta_L^{(3)}} + \alpha_a\Gamma_a\ddot{\boldsymbol{\theta}}_{\boldsymbol{L}} + \alpha_v\Gamma_v\dot{\boldsymbol{\theta}}_{\boldsymbol{L}} + \boldsymbol{v_r}, \tag{23}$$

where the coefficients Γ_j, Γ_a and Γ_v are defined in (10) and α_j, α_a and α_v are scalars between [0, 1]. The closed loop system is given by

$$\begin{bmatrix} Q_c(s) & X(s)s \\ -I & \Lambda_L(s) \end{bmatrix}\begin{bmatrix} \boldsymbol{\tau}_L \\ \boldsymbol{\theta}_L \end{bmatrix} = \begin{bmatrix} K_p(s + K_i) \\ 0 \end{bmatrix}\boldsymbol{\tau}_r + \begin{bmatrix} (Ls + R)K_t^{-1}\boldsymbol{\tau}_d \\ \boldsymbol{\tau_{Ld}} \end{bmatrix} \tag{24}$$

From (23), $F(s) = \alpha_j\Gamma_j s^3 + \alpha_a\Gamma_a s^2 + \alpha_v\Gamma_v s$ and using (8) we arrive at $X(s) = (1 - \alpha_j)\Gamma_j s^3 + (1 - \alpha_a)\Gamma_a s^2 + (1 - \alpha_v)\Gamma_v s$.

Lemma 6 *The closed loop characteristic polynomial of* (24) *is given by*

$$\det(Q_c(s)\Lambda_L(s) + X(s)s) = 0 \tag{25}$$

Proof. From (24) the determinant of the block partitioned matrix is

$$\det(Q_c(s))\det(\Lambda_L(s)+Q_c^{-1}(s)X(s)s) = \det(Q_c(s))\det\left(Q_c^{-1}(s)\{Q_c(s)\Lambda_L(s)+X(s)s\}\right) \quad (26)$$

$$= \det(Q_c(s))\det(Q_c^{-1}(s))\det(Q_c(s)\Lambda_L(s)+X(s)s) \quad (27)$$

But $\det(Q_c(s))\det(Q_c^{-1}(s)) = 1$ and this gives (25).

■

Remark 2: Expanding (25) in powers of s we can obtain a state space realization of $(Q_c(s)\Lambda_L(s)+X(s)s)$ in terms of block companion matrix and compute the corresponding eigenvalues to determine stability of the closed loop system (24). The block companion form is given in 8.

2.5 *Disturbance Rejection*

This section provides the main result to asses the disturbance rejection properties of the closed loop system with a PI torque controller for both the full positive feedback compensation and a partial compensation. The disturbances of interest are $\boldsymbol{\tau_d}$ those occurring at the motor since these can represent nonlinear friction and torque ripples in the gearbox.

Lemma 7 Disturbance Transmission

1. *For the closed loop system in lemma 5 with full feedback compensation the transfer function matrix from $\boldsymbol{\tau_d}$ to the joint torque $\boldsymbol{\tau_L}$ is*

$$\boldsymbol{\tau_L} = Q_c^{-1}(s)(Ls+R)K_t^{-1}s\boldsymbol{\tau_d} \quad (28)$$

2. *For the closed loop system (24) with a partial feedback compensation the transfer function matrix from $\boldsymbol{\tau_d}$ to the joint torque $\boldsymbol{\tau_L}$ is*

$$\boldsymbol{\tau_L} = [I+Q_c^{-1}(s)X(s)\Lambda_L^{-1}(s)s]^{-1}Q_c^{-1}(s)(Ls+R)K_t^{-1}s\boldsymbol{\tau_d} \quad (29)$$

Proof. Equation (28) in part 1 follows easily by setting $\boldsymbol{\tau_r} = 0$ in (20). For (29) in part 2 setting $\boldsymbol{\tau_r} = 0$ in (24) and using the inverse of a block partitioned matrix we have

$$\begin{aligned}\boldsymbol{\tau_L} &= [Q_c(s)+X(s)\Lambda_L^{-1}(s)s]^{-1}(Ls+R)K_t^{-1}s\boldsymbol{\tau_d}\\ &= [Q_c(s)(I+Q_c^{-1}(s)X(s)\Lambda_L^{-1}(s)s)]^{-1}(Ls+R)K_t^{-1}s\boldsymbol{\tau_d}\\ &= [I+Q_c^{-1}(s)X(s)\Lambda_L^{-1}(s)s]^{-1}Q_c^{-1}(s)(Ls+R)K_t^{-1}s\boldsymbol{\tau_d}\end{aligned}$$

■

From (28) and (29) the disturbance rejection properties of the linearized system can be displayed via the relevant frequency response plots. This will be illustrated in section 3 for the two DoF example.

3 Case Study

In this section a two DoF nonlinear model is used as a case study to show the improved torque performance with PI controllers combined with the positive feedback (12). Model parameter values are given in section 3.1. Nonlinear simulations are presented in sections 3.2 and 3.3, while section 3.4 discusses how the load stiffness K_L affects the transmission zeros. Also, the effects on closed loop stability when ignoring jerk and acceleration in the positive feedback are investigated. It is shown that to maintain stability jerk and acceleration feedback terms in general cannot be discarded except for some particular cases.

3.1 *Model and Controller Descriptions*

Parameter values for the two DoF model are provided in this section. The mass-inertia matrix M_L, Coriolis C_L and gravity G vectors are given in relative coordinates:

$$M_L(\boldsymbol{\theta}_L) = \begin{bmatrix} 0.3047 + 0.1908\cos(\theta_{L2}) & 0.0871 + 0.0954\cos(\theta_{L2}) \\ 0.0871 + 0.0954\cos(\theta_{L2}) & 0.0871 \end{bmatrix}, \tag{30}$$

$$C_L(\dot{\boldsymbol{\theta}}_L, \boldsymbol{\theta}_L) = \begin{bmatrix} -0.0954(2\dot{\theta_{L1}}\dot{\theta_{L2}} + \dot{\theta_{L2}}^2)\sin(\theta_{L2}) \\ 0.0954\ \dot{\theta_{L1}}^2 \sin(\theta_{L2}) \end{bmatrix},\ G(\boldsymbol{\theta}_L) = \begin{bmatrix} 6.6438\sin(\theta_{L1}) + 1.034\sin(\theta_{L1} + \theta_{L2}) \\ 1.034\sin(\theta_{L1} + \theta_{L2}) \end{bmatrix}. \tag{31}$$

The linearized gravity matrix at $\boldsymbol{\theta_L}$ is

$$K_L = \begin{bmatrix} 6.6438\cos(\theta_{L1}) + 1.034\cos(\theta_{L1} + \theta_{L2}) & 1.0340\cos(\theta_{L1} + \theta_{L2}) \\ 1.0340\cos(\theta_{L1} + \theta_{L2}) & 1.0340\cos(\theta_{L1} + \theta_{L2}) \end{bmatrix}. \tag{32}$$

Substituting the operating point $\boldsymbol{\theta_L} = [0, 0.5]^T$ and $\dot{\boldsymbol{\theta}}_{\boldsymbol{L}} = [0, 0]^T$ in the linearized model (30) - (32) yields

$$M_L = \begin{bmatrix} 0.4721 & 0.1708 \\ 0.1708 & 0.0871 \end{bmatrix},\ C_L = \begin{bmatrix} 0 \\ 0 \end{bmatrix},\ K_L = \begin{bmatrix} 7.5512 & 0.9074 \\ 0.9074 & 0.9074 \end{bmatrix}. \tag{33}$$

The analysis can be repeated at other operating points θ_L. Identical drives are used for each DoF in this system. A harmonic drive gearbox with stiffness $K_H = 912I\ [\frac{Nm}{rad}]$ and reduction ratio $N = 150I$. A motor with inductance $L = 3.2\ 10^{-4}I\ [H]$, resistance $R = 0.664I\ [\Omega]$, torque constant and back EMF constant $K_t = K_\omega = 0.041I\ [\frac{V.sec}{rad}]$. The total drive inertia, $J_m = 1.387\ 10^{-5}I\ [Kg.m^2]$ and damping $Bm = 1.996\ 10^{-5}I\ [\frac{V.sec}{rad}]$. The load damping is $B_L = 0.01I\ [\frac{V.sec}{rad}]$.

Decentralized PI torque controllers were designed using the result in Lemma 5 and the Routh-Hurwitz inequalities (21) and (22). Fig.2 shows the stability region for the controller gains, where the maximum value for k_p is 14. In addition, the controller gains were also selected so that the closed loop system without positive feedback is also stable. The controllers are given by

$$G_c(s) = k_o \begin{bmatrix} \frac{(s+12.5)}{s} & 0 \\ 0 & \frac{(s+25)}{s} \end{bmatrix}, \tag{34}$$

where $k_o \in [0\ 6]$. The controller gain $k_o = 2$ is chosen to achieve a closed loop torque bandwidth of 50 Hz (settling time of about 45 $msec$) and overshoot of 30% at each joint after applying the positive feedback (12).

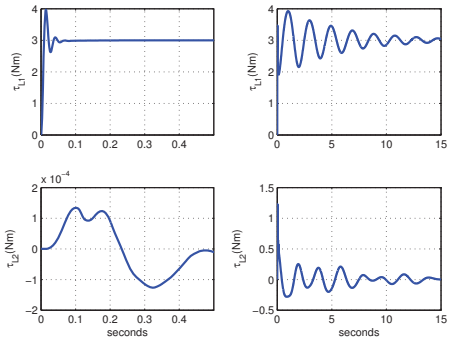

Figure 3: Torque step responses of nonlinear closed loop system with positive feedback (left) and without positive feedback (right)

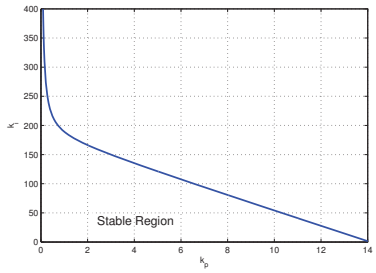

Figure 2: Stability region for the PI torque controller gains.

3.2 *Nonlinear Simulation Results*

This section presents simulation results comparing the closed loop performance with and without positive feedback for the PI torque controller (34) and $k_o = 2$. Equations (16) and (17) are used in the nonlinear simulations to compute the load acceleration and jerk terms in the positive feedback.

Fig.3 shows closed loop simulation results of the nonlinear system for a torque step command of $\boldsymbol{\tau_r} = [3,\ 0]^T$. A fast response is achieved with positive feedback compensation as seen in the left hand side plots in Fig.3 while the step response shown in the right hand side without the positive feedback has a long transient and is oscillatory. It is evident that the positive feedback has considerably improved the torque tracking bandwidth. However Fig.4 shows that the control signals for the system with positive feedback are more responsive to load motion.

3.3 *Disturbance Rejection*

In this section, the disturbance rejection properties of the proposed controller are analyzed in terms of bode plots for the closed loop system using the results from

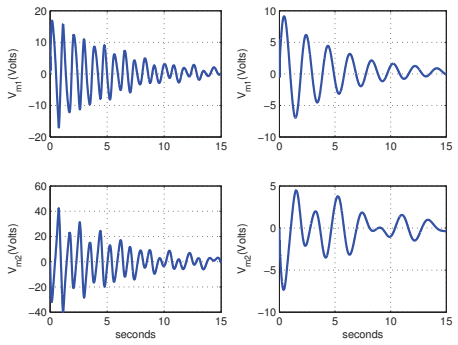

Figure 4: Motor voltages for torque step responses of nonlinear closed loop system with positive feedback (left) and without positive feedback (right)

Lemma 7. In particular it is shown that the linearized analysis can predict with reasonable accuracy the amplitudes of oscillations caused by cyclic friction $\boldsymbol{\tau_d}$ at the motor input. The predicted amplitudes match well the oscillations observed in nonlinear simulations. In general, nonlinear friction and torque ripples cause undesirable effects in the closed loop response of mechanical systems which may be reduced by increasing the bandwidth of the closed loop system or designing suitable friction compensation schemes. In particular, torque ripples or cyclic friction in gearboxes give rise to oscillations [21] [22]. These disturbances are then propagated throughout the system.

Fig.5 shows the step response nonlinear simulation of the closed loop system with cyclic friction included in both motors. The torque reference for joint one is 3 Nm and zero for joint two. Full positive feedback is applied together with the PI torque controller. The RMS torque errors are 0.0961 Nm and 0.0725 Nm for the first and second DoFs respectively. The torque ripple used at the input of the motors is $\boldsymbol{\tau_d} = 0.013\cos(2\boldsymbol{\theta_m} + \boldsymbol{\phi})\ Nm$ where $\boldsymbol{\phi} = \pi$ for joint one and $\boldsymbol{\phi} = \frac{\pi}{2}$ for joint two. The amplitude and phase of the torque ripples were estimated from experimental data for a drive mounted on a single joint system and corresponds to the fundamental frequency of the ripples arising in the harmonic drive [21]. Similar models for cyclic friction have been reported in [22] for other types of gearboxes.

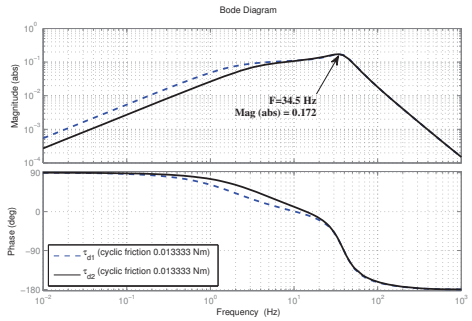

Figure 6: Bode plot of joint torque with torque ripple disturbance for the two DoF system. The peak magnitude is about 35 Hz.

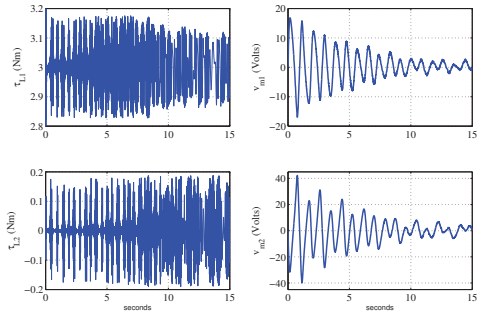

Figure 5: Joint torque step response with torque ripple disturbance and the corresponding control input for a two DoF system.

The bode plots in Fig.6 show how the disturbances $\boldsymbol{\tau_d}$ affect the joint torque. The worst case is the resonance at 35 Hz while all other frequencies are attenuated much further. Note that the peak amplitude in the bode plot predicts quite well the oscillation peaks in the nonlinear simulation shown in Fig.3. The power spectral density of the torque oscillation errors due to cyclic friction is shown in Fig.7. The figure clearly shows that peak values occur in the frequency range $30 - 40$ Hz which is in the neighborhood of resonant peak in the bode plot.

3.3.1 *Resonance Compensation*

There are several options to reduce the effect of torque ripples, for example using lead or notch compensators in cascade with the PI controllers. For the nonlinear simulation shown in Fig.8, a lead compensator $G_{LC}(s) = (\frac{628}{128})\frac{s+128}{s+628}$ is added in cascade with the PI controller. The simulation clearly shows a substantial reduction in the peak amplitude of the oscillations to about 0.1. The RMS

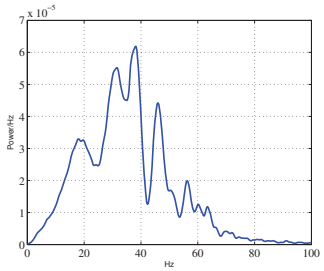

Figure 7: Power spectrum of joint torque error response for the two DoF system. The peak magnitudes occur around 35 Hz.

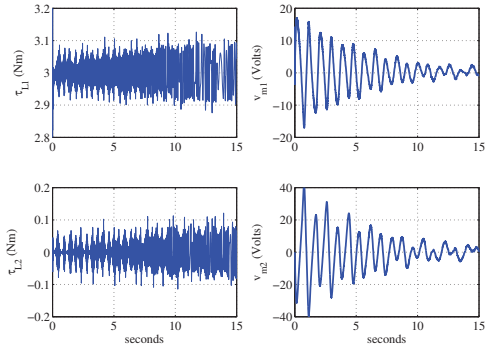

Figure 8: Joint torque step response with torque ripple disturbance and the corresponding control input with lead compensation.

torque errors have been reduced to 0.0640 Nm for joint one and 0.0391 Nm for joint two. The resulting bode plot in Fig.9 also shows the effectiveness of the lead compensator which has attenuated all the magnitudes to less than 0.091.

Stiction is another disturbance which is present in torque control problem. Fig.10 shows the effect of stiction before and after lead compensation. The simulations show that also the effects of stiction are reduced for the controller with the lead compensator. If disturbance rejection cannot be improved with PI controllers and simple additional compensators then more complex controllers are needed. This highlights some limitations when using PI control.

3.4 *Transmission Zeros and Approximate Positive Feedback*

This section first considers how load stiffness K_L and damping B_L affect the transmission zeros location in the complex plane. Then the effects of approximate positive feedback on pole-zero cancellations and closed loop stability are

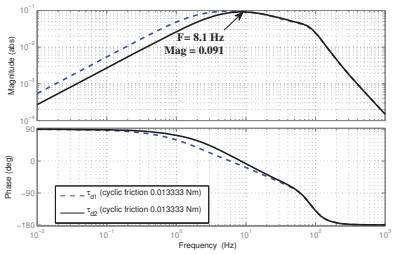

Figure 9: Bode plot of joint torque with ripple disturbance for the two DoF system with lead compensation.

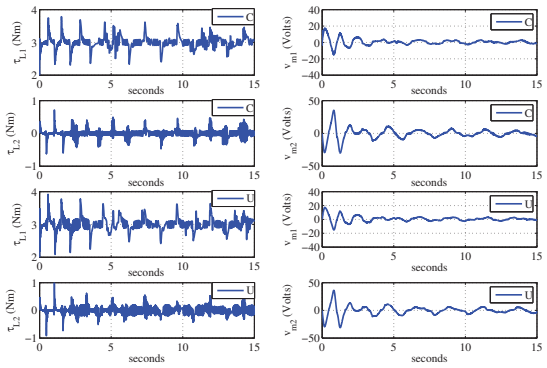

Figure 10: Torque step responses of lead compensated (C) and uncompensated (U) system with cyclic friction and stiction.

investigated, in particular when the load acceleration and jerk terms in the positive feedback are neglected.

3.4.1 Effect of Load Stiffness and Damping on Transmission Zeros

This section presents a discussion regarding load stiffness K_L and damping B_L effects on the multivariable zeros. The two DoF case study is used to illustrate these effects numerically. Throughout it is assumed that B_L is positive definite.

First consider the case when the load stiffness is positive definite, $K_L > 0$. In this case the transmission zeros will always lie in the open left half plane and when damping is small these zeros will be located near the imaginary axis. For the linearized system (33) there are four transmission zeros, the roots of $\det(\Lambda_L(s) = 0)$, located in complex pairs at $-0.0304 \pm j3.0036$ and $-0.2037 \pm j7.4767$. As B_L increases the zeros move towards the real negative axis. For the case study setting $B_L = diag([0.8,\ 0.4])$ there are two complex zeros $-0.9408 \pm j3.3033$ and two real zeros at -2.4747 and -17.29.

When $K_L = 0$, the linearized system will have as many zeros as degrees of freedom located at the origin. Since M_L and B_L are positive definite, the remaining zeros lie on the negative real axis. The zeros at the origin cancel out with unobservable eigenvalues at the origin. For the case study two zeros at the origin cancel out with two unobservable eigenvalues and the two remaining zeros are at -0.0186 and -0.4496. As B_L increases the zeros on the negative real axis move away from the origin. Note however that, despite the closed loop torque subsystem being stable, the overall system is not internally stable since there are zero eigenvalues that are unobservable form the torque sensor. Finally when K_L is indefinite or negative definite, $K_L \leq 0$, there will be zeros in the right half plane (non-minimum phase zeros). In this case the open loop system is also unstable. If the tw DoF system is linearized at $\boldsymbol{\theta_L} = [\frac{\pi}{2}, \frac{\pi}{2}]^T$ then $K_L = [-1.0340\ \ -1.0340; -1.0340\ \ -1.0340]$ and clearly this is not positive definite (one zero eigenvalue and one negative eigenvalue). There is a zero at the origin which cancels out with an unobservable eigenvalue, the other zeros are at -3.5042, -0.0919 and 3.38893. The open loop system also has and an unstable eigenvalue at 0.0361. Linearizing at $\boldsymbol{\theta_L} = [1.8, 2.1]^T$, gives $K_L = [-2.2601\ \ -0.7506; -0.7506\ \ -0.7506]$ which is negative definite and the system has two minimum phase zeros -3.5034, -2.4371, two non minimum phase zeros at 2.3118 and 3.4511 and two unstable open loop eigenvalues at 0.0077 and 0.0449. In these cases the unstable open loop system could be stabilized via a sate feedback. For the case study a motor position feedback would be sufficient. However taking into account that state feedback does not change the system zeros the stabilized system still would have non-minimum phase zeros and trying to cancel the non-minimum phase zeros using positive feedback is not feasible since exact pole-zero cancellations will not take place in practice.

An alternative is to consider gravity compensation methods to remove the gravity torque G in the nonlinear system. Gravity compensation methods for systems with flexible joints have been investigated in [23] [24] and are based on the desired gravity compensation (in terms of the desired load position) or using

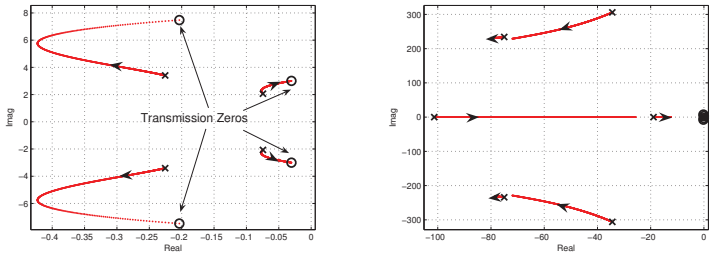

(a) Zoom on the transmission zeros. (b) Overall view of the root locus.

Figure 11: Root locus plot as the positive feedback varies, $\alpha \in [0,\ 1]$, for the PI controller gain $k_0 = 2$

a motor biased compensation. However these methods are only approximate and do not completely remove the gravity torques. Methods employing the actual load position for gravity compensation could be used but these have not been studied in detail and at present we cannot ensure that this is a suitable approach in conjunction with the positive feedback scheme for torque control, particularly for systems that give rise K_L being indefinite or negative definite. This question is left open for future research. Therefore when $K_L \leq 0$ the positive feedback compensation does not seem to be a suitable strategy for torque control.

3.4.2 Effect of Approximate Positive Feedback on Stability

This section considers approximate implementations of the positive feedback compensation for the two DoF case study. In particular, we investigate the effects on closed loop stability when ignoring terms involving load acceleration and jerk.

First consider the positive feedback in (23) and let $\alpha = \alpha_j = \alpha_a = \alpha_v$, where α takes values in the interval $[0,\ 1]$. In this analysis the acceleration and jerk are computed from equations (18)-(19) written in state feedback form. For $\alpha = 0$ there is no positive feedback applied while for $\alpha = 1$ the full compensation is used. For intermediate values of α, a partial positive feedback compensation is implemented. The closed loop poles are given by the roots of the characteristic polynomial in Lemma 6. As α varies, Fig.11(a) and 11(b) show the root locus of the closed loop poles for the two DoF system and the PI controller gain $k_0 = 2$ in (34). The position of the transmission zeros are shown as circles and the poles are shown as crosses. Fig.11(a) displays the root locus in the vicinity of the transmission zeros and for $\alpha = 1$ four poles cancel the four zeros. Fig.11(b) shows an overall view of the root locus. From this analysis we conclude that the closed loop two DoF system with the PI controller remains stable for all $\alpha \in [0,\ 1]$.

Neglecting the jerk term :

Consider the positive feedback (23) with $\alpha_a = \alpha_v = 1$ and $\alpha_j = 0$ so that

the term involving jerk is removed. Using Lemma 6 the effect of discarding jerk feedback is investigated. For the two DoF case study, Fig.12(a) and 12(b) display the root locus plot around the transmission zeros without the jerk feedback term and varying the PI gain k_o in the interval $[0,\ 6]$. In Fig.12(b) it can be seen that the angle of departure from the pole is towards the unstable region but the pole is quickly drawn toward the transmission zero. In this case, ignoring the jerk term does not produce an unstable closed loop system. This result can also be verified for the nonlinear system via a simulation.

Unfortunately this conclusion does not hold in general and we next provide an example showing that without jerk feedback instability can arise. For the two DoF system, $K_L > 0$ and B_L is very small. Now suppose that a motor with a different and larger electrical time constant was chosen, for example if the inductance L was larger by a factor of ten. In this case varying the PI gains k_o in the interval $[0,\ 0.6]$ we arrive at a conditionally stable system [1]. Stability without jerk feedback could be recovered if the damping B_L were sufficiently large, for example if $B_L = \text{diag}[0.1,\ 0.1]$). In summary, when $K_L > 0$, there are cases in which jerk feedback cannot be discarded and Lemma 6 can be used to investigate this issue.

When the load stiffness $K_L = 0$, numerous nonlinear simulations without jerk feedback have not shown stability problems. However a proof for this conjecture is left as an open question. Recall that for $K_L = 0$, the transmission zeros lie on the real negative axis as opposed to the complex zeros presented in section 3.4.1. It seems that in this situation it is easier to compensate the effect of load motion without jerk feedback.

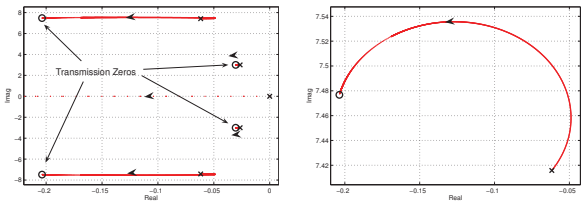

(a) Root locus near transmission zeros.

(b) Root locus near one zero.

Figure 12: Root locus plot of the approximate positive feedback near the transmission zeros, without jerk feedback and varying the PI torque controller gain k_o in the interval $[0,\ 6]$

Neglecting jerk Γ_j and acceleration Γ_a :
Consider the positive feedback (23) with $\alpha_v = 1$ and $\alpha_a = \alpha_j = 0$ so that the terms involving acceleration and jerk are removed. Using Lemma 6 the effect of discarding these terms is investigated. First consider the two DoF case study, when $K_L > 0$ and B_L is very small. In the root locus plot shown in Fig.13 it

[1] Conditional Stability: A conditionally stable system switches between stable an unstable operation as the loop gain varies.

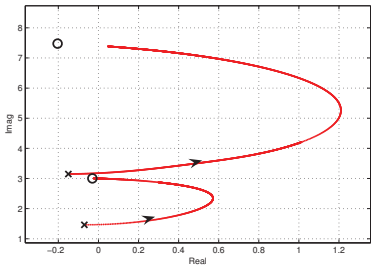

Figure 13: Root locus plot of the approximate positive feedback near transmission zeros, without jerk and acceleration feedback and varying the PI torque controller gain $k_o \in [0,\ 6]$.

can be seen that the angles of departure from the poles are toward the unstable region and the system is conditionally stable. Instability occurs for PI gains k_o in the intervals $(0.00073,\ 7.5196)$ and $k_o > 12.53$. Stability can be restored by further increasing the gain k_o but then performance becomes quite oscillatory because other poles get close to the imaginary axis. When $K_L > 0$ and B_L is sufficiently large, for example if $B_L = \text{diag}\{0.8, 0.4\}$, then the close loop system without acceleration and jerk feedback remains stable as shown in Fig.14(a). In summary, when $K_L > 0$, there are cases in which acceleration and/or jerk feedback cannot be discarded. This can be investigated using Lemma 6. Finally, when $K_L = 0$ the system without acceleration and jerk feedback appears to remain stable. This conjecture is left open for future research.

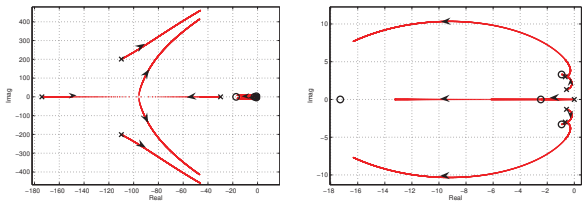

(a) Overall root locus. (b) Zoomed area near the origin.

Figure 14: Root locus plot of the approximate positive feedback without jerk and acceleration feedback for larger damping B_L and varying the PI torque controller gain $k_o \in [0,\ 6]$.

4 Experimental Results

The proposed positive feedback and lead compensation was implemented on the robotic prototype leg presented in [14], and shown in Fig.15 to verify the theoretical results. A 3.6 kg weight was attached at the leg end-effector (center

of mass at 0.42 m from the center of rotation including the mass of the lower leg) to increase the gravity load and permit a reasonable torque step magnitude. The prototype robotic leg used has two actuators (M_1 and M_2) which both move the knee joint while the hip is un-actuated. In this experiment the second actuator M_2 which applies assistive torque at the knee using a bungee cord was removed and only the main knee motor M_1 was used for the experimental verification. Moreover, the hip joint was mechanically locked and the leg was tested while fixed above the ground on the supporting frame. In the experiments a torque step of 3 Nm was applied and the results are presented as follows. The torque signal is measured using two 19 bit encoders measuring the deflection of a torsion bar with known stiffness (930 $\frac{Nm}{rad}$), connected between the gearbox output and the link output. The estimated value of joint damping B_L is 1.5 for the leg. Note that this value of B_L is much larger than the joint damping used in the simulation study presented in section 3. The PI controller $G_c(s) = \frac{2(s+10)}{s}$ was designed to have 46 Hz closed loop bandwidth with full positive feedback. The closed loop system also remains stable for the same PI controller without positive feedback compensation but the closed loop bandwidth is substantially reduced to 0.7 Hz. The velocity is obtained using a 3rd order Butterworth filter with cut-off frequency of 50 Hz and the acceleration and jerk are obtained with first order differentiation of the velocity and acceleration respectively.

Fig.16 compares the system's torque step response in four cases. The step torque reference (τ_r) is applied at $t = 0.4$ *sec.* First, part (a) in Fig. 16 shows the closed loop step response without positive feedback. Second, in part (b) the same PI controller is used with positive velocity feedback $\Gamma_v = 6.909329$. Third, part (c) the PI controller is used with positive velocity and acceleration feedback $\Gamma_a = 0.054354$. Finally, in part (d) the same PI controller is used with full positive feedback proposed in Lemma 2 with positive velocity (Γ_v), acceleration (Γ_a) and jerk feedback $\Gamma_j = 3.975e-5$. The bandwidth of the torque control system with the velocity feedback increases to 46 Hz. As mentioned, since $B_L = 1.5$ is large we can ignore the acceleration and jerk feedback terms without causing instability or degrading closed loop performance.

When using the positive feedback compensation (see Fig.16) the torque settles at the desired value but a 15-20 Hz ripple can be observed which is due to the harmonic drive gearbox friction. This frequency range is shown in the power spectral density graph in Fig. 17. The lead compensator $G_{LC} = \left(\frac{750}{128}\right)\frac{s+128}{s+750}$ is designed to improve disturbance attenuation of the torque ripples and transient response of the torque control. G_{LC} is placed in cascade with the output of the PI controller. Fig.18 depicts the system's torque step response in four cases. The power spectral density plot of the lead compensated torque response is shown in Fig.19. Clearly the magnitude of the oscillations around 15-20 Hz are considerably reduced by 50%.

Figure 15: The prototype robotic leg used in the experiments.

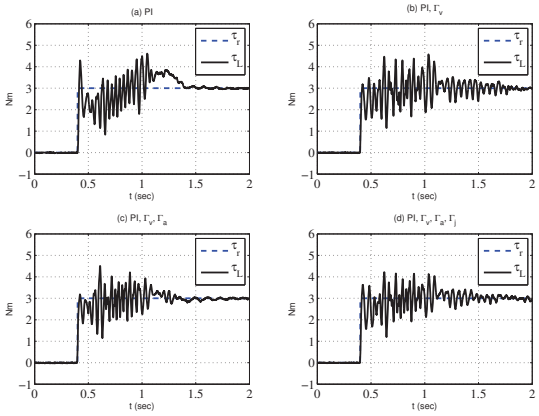

Figure 16: The experimental results of applying the positive feedback of the prototype leg. Torque reference and torque response are shown with dashed, solid lines, respectively. Parts (a), (b), (c) and (d) show the PI control, PI control with velocity compensation, PI control with velocity and acceleration compensation and PI control with velocity, acceleration and jerk compensation, respectively.

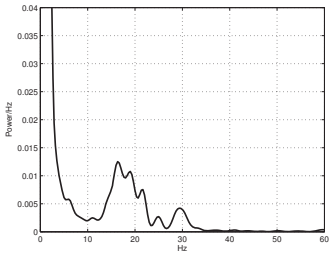

Figure 17: Spectral density plot of the uncompensated (without notch compensation) torque response.

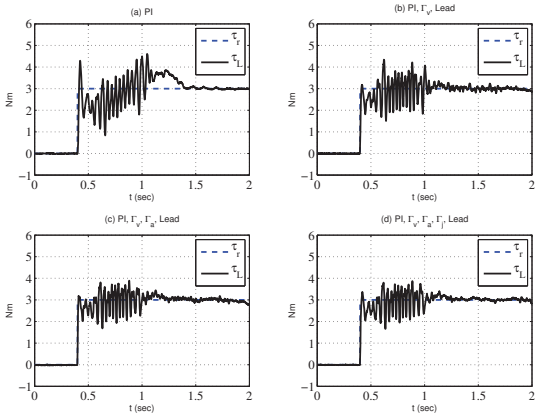

Figure 18: The experimental results of applying the positive feedback with lead compensation of the prototype leg. Torque reference and torque response are shown with dashed, solid lines, respectively. Parts (a), (b), (c) and (d) show the PI control, PI control with velocity and lead compensation, PI control with velocity, acceleration and lead compensation and PI control with velocity, acceleration, jerk and lead compensation, respectively.

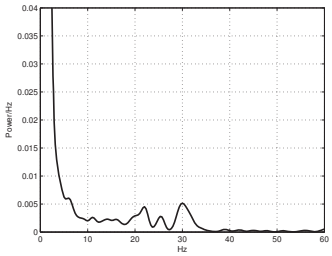

Figure 19: Spectral density plot of the lead compensated torque response.

5 Conclusions

This paper provides a detailed study regarding the use of positive feedback to improve torque control in flexible joint robots driven by electrical actuators. It is shown that torque control bandwidth limitations depend on the load dynamics and a positive feedback scheme can be obtained to improve torque tracking for robots with electrical actuators. A two DoF nonlinear system is used as an example to illustrate torque tracking improvements that can be achieved with positive feedback and simple PI controllers. Approximate positive feedback implementations are also considered and closed loop stability is analyzed using root locus methods. Simulations and experimental results for a prototype robot are shown to confirm the theoretical results.

6 MIMO Transmission Zeros

The linearized system equations can be written in matrix form

$$W(s) \begin{bmatrix} \boldsymbol{i} \\ \boldsymbol{\theta}_m \\ \boldsymbol{\theta}_L \end{bmatrix} = B\, \boldsymbol{v_m} \tag{35}$$

where,

$$W(s) = \begin{bmatrix} Ls + R & K_\omega\, s & 0 \\ -K_t & \Lambda_1(s) & -N^{-1}K_H \\ 0 & -K_H N^{-1} & \Lambda_L(s) + K_H \end{bmatrix}, B = \begin{bmatrix} I \\ 0 \\ 0 \end{bmatrix} \tag{36}$$

$\Lambda_1(s) = \Lambda_m(s) + N^{-1}K_H N^{-1}$, $\Lambda_m(s) = J_m s^2 + B_m s$, $\Lambda_L(s) = M_L s^2 + B_L s + K_L$ and K_L includes the linearized gravity torques. The system matrix $P(s)$ is defined as

$$P(s) = \begin{bmatrix} W(s) & -B \\ C & 0 \end{bmatrix} \tag{37}$$

The system zeros are the values s_0 where $P(s_0)$ looses rank, that is

$$\text{rank}(P(s_0)) < n + \min(\text{rank}(C), \text{rank}(B)$$

where n is twice the number of DoF. The system zeros include the transmission zeros and input/output decoupling zeros. When the system is controllable and observable there are no input/output decoupling zeros. In the transfer function matrix, input/output decoupling zeros cancel out with uncontrollable and/or unobservable poles.

We need to show that $P(s)$ looses rank iff $\det(M_L s^2 + B_L s + K_L) = 0$. To accomplish this we carry out a series of elementary transformation of the system matrix $P(s)$. These transformations amount to post-multiply and/or pre-multiply $P(s_0)$ by a series of unimodular matrices. A unimodular matrix is a square polynomial matrix that has a constant (non-zero) determinant. The

inverse of a unimodular matrix is also a unimodular matrix.
Let $\tilde{P}(s) = Q_1(s)P(s)Q_2(s)$,

$$Q_1(s) = \begin{bmatrix} I & 0 & 0 & 0 \\ 0 & I & 0 & 0 \\ 0 & 0 & I & I \\ 0 & 0 & 0 & K_H^{-1} \end{bmatrix} \tag{38}$$

and

$$Q_2(s) = \begin{bmatrix} -K_t^{-1} & 0 & 0 & 0 \\ 0 & I & 0 & 0 \\ 0 & 0 & I & 0 \\ -(Ls+R)K_t^{-1} & K_\omega s & 0 & -I \end{bmatrix} \begin{bmatrix} I & -\Lambda_1(s)N & -\Lambda_1(s)N + N^{-1}K_H & 0 \\ 0 & N & N & 0 \\ 0 & 0 & I & 0 \\ 0 & 0 & 0 & I \end{bmatrix} \tag{39}$$

Then

$$\tilde{P}(s) = \begin{bmatrix} 0 & 0 & 0 & I \\ I & 0 & 0 & 0 \\ 0 & 0 & \Lambda_L(s) & 0 \\ 0 & I & 0 & 0 \end{bmatrix} \tag{40}$$

It is clear that $Q_1(s)$ and $Q_2(s)$ are unimodular matrices and therefore $P(s)$ and $\tilde{P}(s)$ are equivalent. It is also evident that $\tilde{P}(s)$ looses rank iff $\Lambda_L(s)$ looses rank and this in turn is equivalent to the condition $\det(\Lambda_L(s)) = 0$.

7 Proof of Lemma 2

The plant output torque is given by

$$\boldsymbol{y} = C \begin{bmatrix} \boldsymbol{i} \\ \boldsymbol{\theta_m} \\ \boldsymbol{\theta_L} \end{bmatrix} \tag{41}$$

where $C = [0 \;\; K_H N^{-1} \;\; -K_H]$. Converting (36) in terms of torque $\boldsymbol{\tau}_L$ gives

$$W(s) \begin{bmatrix} \boldsymbol{i} \\ \boldsymbol{\theta}_m \\ \boldsymbol{\theta}_L \end{bmatrix} = W(s) \begin{bmatrix} I & 0 & 0 \\ 0 & NK_H^{-1} & N \\ 0 & 0 & I \end{bmatrix} \begin{bmatrix} \boldsymbol{i} \\ \boldsymbol{\tau}_L \\ \boldsymbol{\theta}_L \end{bmatrix} = B\, \boldsymbol{v_m} \tag{42}$$

Let,

$$\boldsymbol{v_m} = F(s)\boldsymbol{\theta_L} + \boldsymbol{v_r}, \tag{43}$$

Then (35), (36), (42) and (43) yield

$$\begin{bmatrix} (Ls+R) & (K_\omega N K_H^{-1} s) & (K_\omega N s - F(s)) \\ -K_t & (\Lambda_1(s) N K_H^{-1}) & (\Lambda_1(s)N - N^{-1}K_H) \\ 0 & -I & \Lambda_L(s) \end{bmatrix} \begin{bmatrix} \boldsymbol{i} \\ \boldsymbol{\tau}_L \\ \boldsymbol{\theta}_L \end{bmatrix} = B\, \boldsymbol{v_r} \tag{44}$$

From (44) solving for the motor current $\boldsymbol{i}$, substituting in the equation for the torque $\boldsymbol{\tau_L}$ and pre-multiplying by $(Ls+R)K_t^{-1}$ yields

$$\begin{bmatrix} ((Ls+R)K_t^{-1}\Lambda_1(s) + K_\omega s) N K_H^{-1} & (Ls+R)K_t^{-1}\Lambda_m(s)N + K_\omega N s - F(s) \\ -I & \Lambda_L(s) \end{bmatrix} \begin{bmatrix} \boldsymbol{\tau}_L \\ \boldsymbol{\theta}_L \end{bmatrix} = \begin{bmatrix} \boldsymbol{v_r} \\ 0 \end{bmatrix} \tag{45}$$

8 Block Companion Matrix

Consider a polynomial matrix $P(s) = P_n s^n + P_{n-1}s^{n-1} + ... + P_1 s + P_0$ where P_i and $p \times p$ constant matrices and P_n is invertible. A block companion matrix

representation of $P(s)$ is

$$A = \begin{bmatrix} 0 & I & 0 & 0 & 0 & 0 \\ 0 & 0 & I & 0 & 0 & 0 \\ \vdots & \vdots & \vdots & \vdots & \vdots & \vdots \\ 0 & 0 & 0 & 0 & 0 & I \\ -P_n^{-1}P_0 & -P_n^{-1}P_1 & -P_n^{-1}P_2 & \cdots & -P_n^{-1}P_{n-2} & -P_n^{-1}P_{n-1} \end{bmatrix}$$

where 0 and I are $p \times p$ zero and identity matrices respectively.

References

[1] H Vallery, R Ekkelenkamp, H Van Der Kooij, and M Buss, *Passive and accurate torque control of series elastic actuators*, in IEEE/RSJ International Conference on Intelligent Robots and Systems, IROS, pp. 3534-3538, 2007.

[2] G.A. Pratt, M.M. Williamson, *Series elastic actuators*, in IEEE/RSJ International Conference on Intelligent Robots and Systems, 'Human Robot Interaction and Cooperative Robots', vol.1, pp. 399-406, 5-9 Aug 1995.

[3] G.A. Pratt and M.M. Williamson, *Stiffness Isn't Everything,* Fourth International Symposium on Experimental Robotics, 1995.

[4] S. Dyke, B. Spencer Jr., P. Quast, and M. Sain, *Role of control-structure interaction in protective system design*, Journal of Engineering Mechanics, ASCE, vol. 121 no.2, pp. 322-38, 1995.

[5] A. Alleyne, R. Liu and H. Wright, *On the limitations of force tracking control for hydraulic active suspensions*, in Proceedings of the American Control Conference, Philadelphia, Pennsylvania, USA, pp. 43-47, 1999.

[6] J. Dimig, C. Shield, C. French, F. Bailey, and A. Clark. *Effective force testing: A method of seismic simulation for structural testing*, Journal of Structural Engineering-Asce, vol. 125, no.9, pp. 1028-1037, 1999.

[7] C. K. Shield, C. W. French, and J. Timm, *Development and implementation of the effective force testing method for seismic simulation of large-scale structures*, Philosophical Transactions of the Royal Society of London Series a-Mathematical Physical and Engineering Sciences, vol. 359 no. 1786, pp. 1911-1929, 2001.

[8] M. Hashimoto, and Y. Kiyosawa, *Experimental study on torque control using Harmonic Drive built-in torque sensors*, Journal of Robotic Systems, vol. 15, no. 8, pp.435–445, 1998.

[9] T. Boaventura, M. Focchi, M. Frigerio, J. Buchli, C. Semini, G. A. Medrano-Cerda, D. G. Caldwell, *On the role of load motion compensation in high-performance force control*, in IEEE International Conference on Intelligent Robots and Systems (IROS), Vilamoura, Algarve, Portugal, pp. 4066-4071, 2012.

[10] C. Semini, N. G. Tsagarakis, E. Guglielmino, M. Focchi, F. Cannella, and D. G. Caldwell, *Design of HyQ - a hydraulically and electrically actuated quadruped robot*, IMechE Part I: J. of Systems and Control Engineering, vol. 225, no. 6, pp. 831-849, 2011.

[11] F. Aghili, M. Buehler, and J. M. Hollerbach, Motion Control Systems with H^{∞} Positive Joint Torque Feedback, IEEE Trans. On Control Systems Technology, vol. 9, no. 5, pp. 685-695, Sept, 2001.

[12] Je Sung Yeon; Jong Hyeon Park, *Practical robust control for flexible joint robot manipulators*, in Proc. of IEEE International Conference on Robotics and Automation, pp. 3377-3382, 19-23 May, 2008.

[13] G. Hirzinger, A. Albu-Schaeffer, M. Haehnle, I. Schaefer, and N. Sporer, *On a new generation of torque controlled light-weight robots*, in Proceedings IEEE International Conference on Robotics and Automation, volume 4, pp. 3356-3363, 2001.

[14] N.G. Tsagarakis, S. Morfey, H. Dallali, G.A. Medrano-Cerda, and D.G. Caldwell, *An Asymmetric Compliant Antagonistic Joint Design for High Performance Mobility*, in Proc. of IEEE/RSJ International Conference on Intelligent Robots and Systems (IROS), pp. 5512-5517, November 3-7, 2013, Tokyo, Japan.

[15] S. Skogestad and I. Postlethwaite I, Multivariable feedback control: analysis and design 2nd ed. Wiley-Blackwell, 2007.

[16] B. A. Levant, Higher-Order Sliding Modes, Differentiation and Output-Feedback Control, Int. J. of Control, vol. 76, nos 9/10, pp. 924-941, 2003.

[17] C. A. Levant and M. Livne, Exact Differentiation of Signals with Unbounded Higher Order Derivatives, IEEE Trans on Automatic Control, vol. 57, no. 4, pp. 1076-1080, April 2012.

[18] E. S. Ibrir, Linear Time-Derivative Trackers, Automatica vol.40, pp. 397-405, 2004.

[19] M. Smaoui, X. Brun and D. Thomasset, High-order sliding mode for an electropneumatic system: A robust differentiatorcontroller design, Int. J. Robust Nonlinear Control, vol. 18, 2008, pp. 481501.

[20] Y.X. Su, C.H. Zheng, Dong. Sun, and BY. Duan, A simple nonlinear velocity estimator for high-performance motion control, IEEE Transactions on Industrial Electronics, vol. 52, no. 4, pp. 1161-1169, 2005.

[21] T. D. Tuttle and W. A. Seering W. A nonlinear model of a harmonic drive gear transmission, IEEE Trans on Robotics and Automation, vol. 12, 1996, pp.368-374.

[22] E. Garcia, P. Gonzalez de Santos and C. Canudas De Wit, Velocity dependence in the cyclic friction arising with gears, Int. J. of Robotics Research, vol.21, 2002. pp.761-771.

[23] P. Tomei, A Simple PD Controller for Robots with Elastic Joints, IEEE Trans on Automatic Control, vol. 36, 1991, pp.1208-1213.

[24] A. De Luca, B. Siciliano, and L. Zollo, PD control with on-line gravity compensation for robots with elastic joints: Theory and experiments. Automatica, vol.41, 2005, pp.1809-1819.